SINTEF
PROCEEDINGS
2

Proceedings of the 12th International Conference on Computational Fluid Dynamics in the Oil & Gas, Metallurgical and Process Industries

Progress in Applied CFD – CFD2017

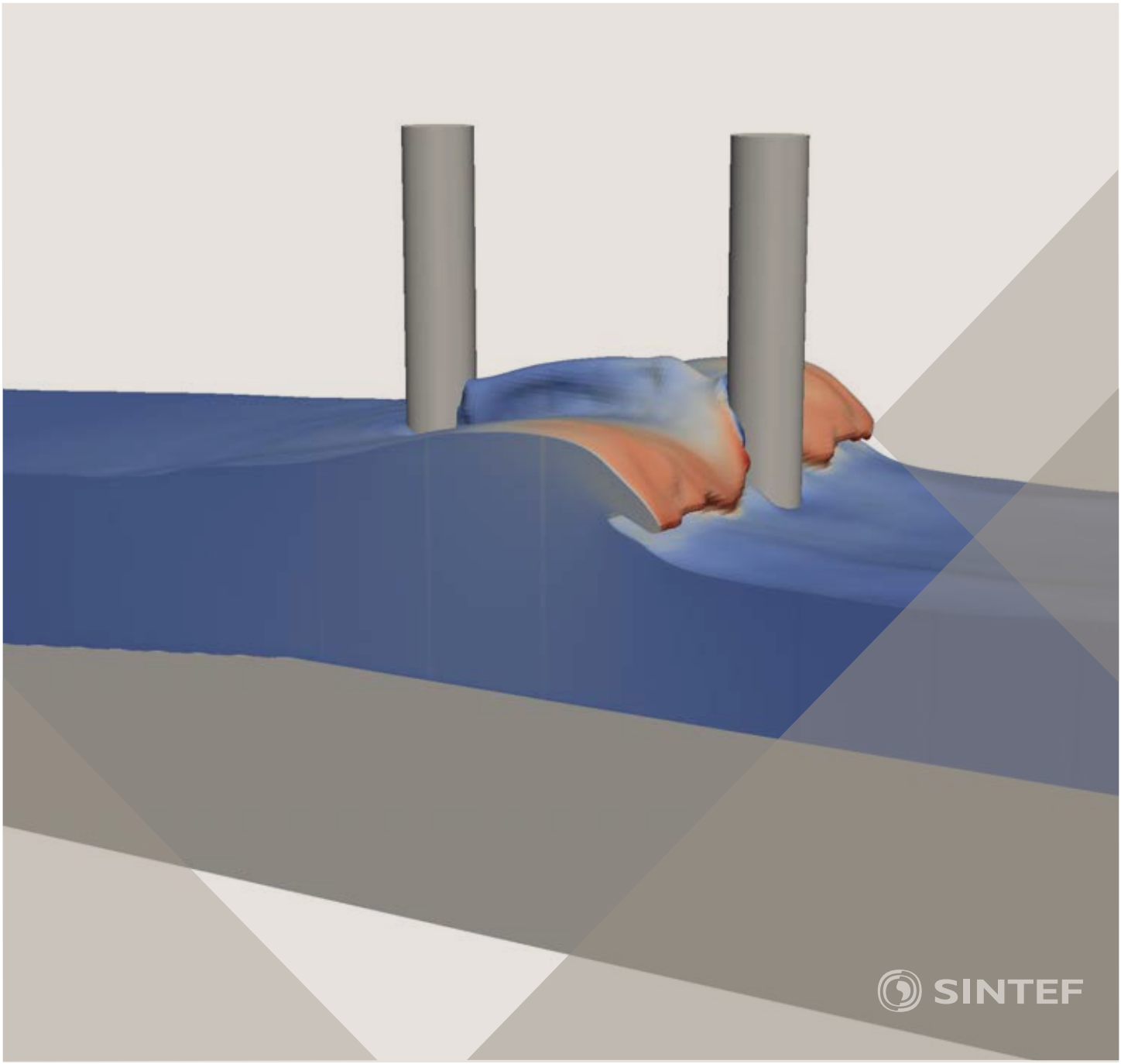

SINTEF Proceedings

Editors:
Jan Erik Olsen and Stein Tore Johansen

Progress in Applied CFD – CFD2017

Proceedings of the 12th International Conference on Computational Fluid Dynamics in the Oil & Gas, Metallurgical and Process Industries

SINTEF Academic Press

SINTEF Proceedings no 2
Editors: Jan Erik Olsen and Stein Tore Johansen
Progress in Applied CFD – CFD2017
Selected papers from 10th International Conference on Computational Fluid Dynamics in the Oil & Gas, Metallurgical and Process Industries

Key words:
CFD, Flow, Modelling

Cover, illustration: Arun Kamath

ISSN 2387-4295 (online)
ISBN 978-82-536-1544-8 (pdf)

SINTEF Academic Press
Address: Forskningsveien 3 B
PO Box 124 Blindern
N-0314 OSLO
Tel: +47 73 59 30 00
Fax: +47 22 96 55 08

www.sintef.no/byggforsk
www.sintefbok.no

SINTEF Proceedings
SINTEF Proceedings is a serial publication for peer-reviewed conference proceedings on a variety of scientific topics.
The processes of peer-reviewing of papers published in SINTEF Proceedings are administered by the conference organizers and proceedings editors. Detailed procedures will vary according to custom and practice in each scientific community.

PREFACE

This book contains all manuscripts approved by the reviewers and the organizing committee of the 12th International Conference on Computational Fluid Dynamics in the Oil & Gas, Metallurgical and Process Industries. The conference was hosted by SINTEF in Trondheim in May/June 2017 and is also known as CFD2017 for short. The conference series was initiated by CSIRO and Phil Schwarz in 1997. So far the conference has been alternating between CSIRO in Melbourne and SINTEF in Trondheim. The conferences focuses on the application of CFD in the oil and gas industries, metal production, mineral processing, power generation, chemicals and other process industries. In addition pragmatic modelling concepts and bio-mechanical applications have become an important part of the conference. The papers in this book demonstrate the current progress in applied CFD.

The conference papers undergo a review process involving two experts. Only papers accepted by the reviewers are included in the proceedings. 108 contributions were presented at the conference together with six keynote presentations. A majority of these contributions are presented by their manuscript in this collection (a few were granted to present without an accompanying manuscript).

The organizing committee would like to thank everyone who has helped with review of manuscripts, all those who helped to promote the conference and all authors who have submitted scientific contributions. We are also grateful for the support from the conference sponsors: ANSYS, SFI Metal Production and NanoSim.

Stein Tore Johansen & Jan Erik Olsen

Organizing committee:

Conference chairman: Prof. Stein Tore Johansen
Conference coordinator: Dr. Jan Erik Olsen
Dr. Bernhard Müller
Dr.Sigrid Karstad Dahl
Dr.Shahriar Amini
Dr.Ernst Meese
Dr.Josip Zoric
Dr.Jannike Solsvik
Dr.Peter Witt

Scientific committee:

Stein Tore Johansen, SINTEF/NTNU
Bernhard Müller, NTNU
Phil Schwarz, CSIRO
Akio Tomiyama, Kobe University
Hans Kuipers, Eindhoven University of Technology
Jinghai Li, Chinese Academy of Science
Markus Braun, Ansys
Simon Lo, CD-adapco
Patrick Segers, Universiteit Gent
Jiyuan Tu, RMIT
Jos Derksen, University of Aberdeen
Dmitry Eskin, Schlumberger-Doll Research
Pär Jönsson, KTH
Stefan Pirker, Johannes Kepler University
Josip Zoric, SINTEF

CONTENTS

A LAGRANGIAN-EULERIAN HYBRID MODEL FOR THE SIMULATION OF DIRECT REDUCTION OF IRON ORE IN FLUIDIZED BEDS

Simon SCHNEIDERBAUER[1*], **Mustafa E. KINACI**[1†], **Franz HAUZENBERGER**[2‡], **Stefan PIRKER**[3§]

[1]Christian-Doppler Laboratory for Multi-Scale Modelling of Multiphase Processes, Johannes Kepler University, 4040 Linz, AUSTRIA

[2]Primetals Technologies Austria GmbH, 4031 Linz, AUSTRIA

[3]Department of Particulate Flow Modelling, Johannes Kepler University, 4040 Linz, AUSTRIA

[*] E-mail: simon.schneiderbauer@jku.at
[†] E-mail: mustafa_efe.kinaci@jku.at
[‡] E-mail: franz.hauzenberger@primetals.com
[§] E-mail: stefan.pirker@jku.at

ABSTRACT

Fluidized bed and moving bed reactors are one of the most important technologies in several branches of process industry. Especially, it is known since decades that iron can be reduced rapidly and efficiently from iron carrier materials using such. The primary energy sources and reducing agents are natural gas, coal, coke, pulverized coal, which are finally released as CO_2 and in a lesser extent as H_2O to the environment. Iron reduction consumes about 70% of the energy during steelmaking therefore offering potential in energy and CO_2 savings. Due to the limited accessibility for measurements, simulation methods have become one of the most important tools for optimizing the iron making processes. While the two-fluid model (Schneiderbauer *et al.*, 2012) would be a good candidate to attack the simulation of large-scale multi-phase processes it lacks from a proper representation of the particle size distribution and the related physical phenomena. This, in turn, gives rise to particle-based approaches, such as the coupling between CFD and DEM methods, which can easily handle particle segregation, particle growth and particle mixing. Furthermore, chemical reactions can be evaluated per particle and it is not required to transfer these reactions to a continuum representation. However, CFD-DEM approaches require an appropriate coarse-graining to considerably reduce their computational demands. We, therefore, present a generalization of the Lagrangian-Eulerian hybrid model for the numerical assessment of reacting poly-disperse gas-solid flows (Schneiderbauer *et al.*, 2016b) to fluidized beds used for iron ore reduction. The main idea of such a modeling strategy is to use a combination of a Lagrangian discrete phase model (DPM) and a coarse-grained two-fluid model (TFM) to take advantage of the benefits of those two different formulations. On the one hand, the DPM model unveils additional information such as the local particle size distribution, which is not covered by TFM. On the other hand, the TFM solution deflects the DPM trajectories due to the inter-particle stresses. This hybrid approach further enables the efficient evaluation of the gas-solid phase reduction of iron ore at a particle level using DPM. The predictive capability and numerical efficiency of this reactive hybrid modeling approach is demonstrated in the case of a lab-scale fluidized bed. The results show that the model is able to correctly predict fractional reduction of the iron ore. The results further give a closer insight about the temperatures and reaction gas consumption due to the reduction process.

Keywords: fluidized bed, iron ore reduction, two-fluid model.

A complete list of symbols used, with dimensions, is required.

NOMENCLATURE

Greek Symbols

β	drag coefficient, $[kg/m^3 s]$
ρ	Mass density, $[kg/m^3]$
ε	volume fraction, (-)
μ_g	viscosity of gas phase, $[Pa\,s]$
τ	Tortuosity, (-)

Latin Symbols

a,b,c	Stoichiometric coefficients of relative species
A,B,C	Species
A_p	Particle surface area, $[m^2]$
C_i	Molar Concentration of species i, $[mol/m^3]$
$D_{j,i}$	Binary gas diffusion, $[m^2/s]$
d	Particle diameter, $[m]$
E_a	Activation energy, $[kJ/mol]$
f_j	Local fractional reduction of the $j^t h$ layer, $[kJ/mol]$
G_Δ	Box filter defined by numerical grid, (-)
k_0	Pre-exponential factor, $[m/s]$
Ke_j	Equilibrium constant of layer j, (-)
k_f	Mass transfer coefficient, $[m/s]$
k_j	Reaction rate constant, $[m/s]$
m_i	Mass of species i, $[kg]$
M_i	Molecular mass of species i, $[kg/mol]$
N_i	Number of moles of species i, $[mol]$
n	Number density, $[1/m^3]$
Nu	Nusselt number, (-)
Pr	Prandtl number, (-)
P_t	Total pressure, $[bar]$
R	Universal gas constant, $[kJ/molK]$
Re	Reynolds number, (-)
r_p	Particle radius, $[m]$
r_j	Layer radius, $[m]$
Sc	Schmidt number, (-)
Sh	Sherwood number, (-)
T	Temperature, $[K]$
u	velocity, $[m/s]$
$\dot{Y}_{i,j}$	Mass fraction of species i layer j, (-)
X_i	Molar fraction of species i, (-)

Sub/superscripts

g	Gas phase
i	species i
j	layer j

s solid phase

INTRODUCTION

The main conversion process to gain metallic iron from oxidic iron compounds is the reduction of iron ores by suitable reducing agents, where iron oxides are reduced to metallic iron by gaseous reducing agents (CO and H_2). During the reduction of iron ores, oxygen is removed accoring to the thermodynamic equlibrium conditions, until the next oxidation level is reached. The gaseous reduction of iron oxides as well as the oxidation of the reducing agents can be described by the following reaction mechanism (Valipour, 2009)

$$\mathrm{Fe}_x\mathrm{O}_y + y\mathrm{CO} \rightleftharpoons x\mathrm{Fe} + y\mathrm{CO}_2, \quad (1)$$

$$\mathrm{Fe}_x\mathrm{O}_y + y\mathrm{H}_2 \rightleftharpoons x\mathrm{Fe} + y\mathrm{H}_2\mathrm{O}. \quad (2)$$

These equations reveal that the reduction reactions of iron ores can be considered as elementary reactions, which means that the number of moles of the gaseous components does not change during the reactions. Thus, the equilibrium of reactions is independent of the total pressure of the reaction system and the chemical equilibrium conditions only depend on temperature.

The leading process used in iron-making is the blast furnace, which consists of a moving bed reactor with countercurrent flow of the solid reactants against a reducing gas. In the lower part the iron is molten and carburized. However, in the blast furnace process iron ore fines, which build up around 80% of the total iron ore, needs to go through a preparation step (i.e. pelletizing or sintering process; Schenk (2011)). In contrast, by using fluidized bed technology fine ores can directly be charged into the reduction process. Such fluidized bed reactors are used, for example, in the FINEX® process (Habermann *et al.*, 2000; Primetals Technologies Austria GmbH and POSCO E&C, 2015). The FINEX® process, which was jointly developed by POSCO (Korea) and Primetals Technologies (Austria), produces hot metal in the same quality as traditional blast furnaces, however the coke making and sintering of the fine ores are avoided. The iron-ores that are charged into the process go through fluidized bed reactors where they are heated and reduced to DRI (Direct Reduced Iron), charged into the melter gasifier, where final reduction and melting as well as the production of reducing gas by gasification of coal with oxygen takes place (Plaul *et al.*, 2009).

Due to the limited accessibility for measurements, simulation methods have become one of the most important tools for optimizing the iron making processes (Valipour, 2009; Natsui *et al.*, 2014; Valipour *et al.*, 2006; Fu *et al.*, 2014). However, either these numerical models neglect the impact of the reduction of iron ore (Fu *et al.*, 2014) or these are restricted to very small scale processes such as, individual pellets (Valipour, 2009; Valipour *et al.*, 2006) or lab-scale fluidized beds (Natsui *et al.*, 2014). It has to be noted that the latter utilized the CFD-DEM approach to model the gas-solid flow, where the continuous phase is governed by computational fluid dynamics (CFD) and the particle trajectories are computed by using the discrete element method (DEM), which is rather computationally demanding (Goniva *et al.*, 2012).

Since the total number of particles in fluidized bed reactors is extremely large, it may be impractical to solve the equations of motion for each particle. It is, therefore, common to investigate particulate flows in large process units using averaged equations of motion, i.e. two-fluid models (TFM), which include the inter-particle collisions statistically by kinetic theory based closures of the particle stresses (Lun *et al.*, 1984; Schneiderbauer *et al.*, 2012; Agrawal *et al.*, 2001). However, each representative particle diameter requires an additional momentum and continuity equation, which considerably raises the computational demand with increasing number of particle diameters (Iddir and Arastoopour, 2005; Schellander *et al.*, 2013). One may restrict the calculations to spatially constant particle size distributions to evaluate the gas-solid drag force (Schneiderbauer *et al.*, 2015a). To overcome this deficiency of TFM, we follow our previous work (Schneiderbauer *et al.*, 2016a; Schellander *et al.*, 2013; Pirker *et al.*, 2010; Schneiderbauer *et al.*, 2015b; Pirker and Kahrimanovic, 2009) and employ a hybrid model for the numerical assessment of poly-disperse gas-solid fluidized beds. The main idea of such a modeling strategy is to use a combination of a Lagrangian discrete phase model (DPM) and a TFM to take advantage of the benefits of those two different formulations. On the one hand, the local degree of polydispersity (i.e. the local particle size distribution), which is essential for the evaluation of the gas-solid drag force, can be obtained by tracking statistically representative particle trajectories for each particle diameter class. On the other hand, the computationally demanding tracking of the inter-particle collisions can be obtained from the inter-particle stresses, which are deduced from the TFM solution. These then appear in addition to the gas-particle drag as a body force in the equation of motion of each DPM-trajectory. Thus, the hybrid model represents a TFM simulation with additional DPM particles, which are used, for example, to provide a closure for the poly-disperse drag law. Finally, by employing the above Lagrangian-Eulerian hybrid model, the reduction of the iron ore as well as the corresponding reaction heat can be computed based on the representative Lagrangian particles. This, in turn, includes the conversion of iron oxides to iron.

In this paper, we employ a Eulerian-Lagrangian hybrid model (Schneiderbauer *et al.*, 2016a,b) to the direct reduction of iron ore in fluidized beds. Here, the reduction is computed based on representative Langrangian trajectories, where the reduction model is based on literature (Hanel *et al.*, 2015; Valipour, 2009; Valipour *et al.*, 2006; Natsui *et al.*, 2014).

POLY-DISPERSE GAS-SOLID FLOWS

Two-fluid model (TFM)

In this work, we used a kinetic-theory based two-fluid model (TFM) to study fluidized beds. Since these equations have been extensively discussed in our previous work (Schneiderbauer *et al.*, 2013, 2012; Schneiderbauer and Pirker, 2014), we do not repeat all the details here and solely present the continuity and momentum equations for the solid phase below:

$$\frac{\partial}{\partial t}\varepsilon_s\rho_s + \nabla\cdot(\varepsilon_s\rho_s u_s) = \mathcal{R}_s, \quad (3)$$

$$\frac{\partial}{\partial t}(\varepsilon_s\rho_s u_s) + \nabla\cdot(\varepsilon_s\rho_s u_s u_s) = -\varepsilon_s\nabla p - \nabla\cdot\left(\boldsymbol{\Sigma}_s^{\mathrm{kc}} + \boldsymbol{\Sigma}_s^{\mathrm{fr}}\right) + \beta(u_g - u_s) + \varepsilon_s\rho_s\boldsymbol{g}. \quad (4)$$

Here, ρ_s, ε_s and $\boldsymbol{u}_s$ denote density, volume fraction and local-average velocity of the solid phase, respectively; $\mathcal{R}_s$ denotes the rate of oxygen removal due to chemical reactions; p is the gas phase pressure; u_g is the local-average velocity of the gas phase; β is the microscopic drag coefficient, which is closed by the poly-disperse drag law of Beetstra *et al.* (2007) (see

table 1); $\boldsymbol{g}$ is the gravitational acceleration; finally, $\boldsymbol{\Sigma}_s^{\mathrm{kc}}$ and $\boldsymbol{\Sigma}_s^{\mathrm{fr}}$ are the stress tensors associated with the solids phase, where the frictional contribution, $\boldsymbol{\Sigma}_s^{\mathrm{fr}}$, arises from enduring or multi-particle collision events in dense areas. The kinetic-collisional part, $\boldsymbol{\Sigma}_s^{\mathrm{kc}}$, is closed using kinetic theory (Hrenya and Sinclair, 1997; Lun *et al.*, 1984), which requires an additional equation for the granular temperature. It has to be further noted that in our previous study (Schellander *et al.*, 2013) we considered an additional term on the right hand side of the solids momentum equation, which accounted for the impact of particle rotation (Magnus force). Particle rotation is assumed to be non-significant in fluidized beds and is therefore included in this work.

Lagrangian discrete phase model (DPM)

We follow our previous work (Schneiderbauer *et al.*, 2016a,b) and obtain the local volume fraction of the different particle size classes $\varepsilon_{s,i} = x_i \varepsilon_s$, which is required for the evaluation of the gas-solid drag force (compare with table 1), by tracking statistically representative particle trajectories for each particle diameter class along the solids flow obtained from TFM. In particular, such a trajectory k represents a_k real particles, which are referred to parcels (Radl and Sundaresan, 2014). Thus, we obtain for the number density of size class i

$$n_i(\boldsymbol{x}) = \sum_{k \in \mathcal{P}_i} a_k G_{\Delta_g}(\boldsymbol{x} - \boldsymbol{x}_{p,k}), \tag{5}$$

which is connected to the volume fraction $\varepsilon_{s,i}$ by

$$\varepsilon_{s,i} = n_i \pi \frac{d_{s,i}^3}{6} \tag{6}$$

yielding

$$x_i = \pi \frac{d_{s,i}^3}{6} \frac{n_i}{\varepsilon_s} \tag{7}$$

In equation (5), Δ_g denotes the grid spacing of the Eulerian grid and the set $\mathcal{P}_i$ contains all parcels of particle size class i. We further obtain the local Sauter diameter, which is required for the evaluation of the drag force and the kinetic theory stresses, from

$$\langle d_s \rangle = \left[\sum_{i=1}^{N_{sp}} \frac{x_i}{d_{s,i}} \right]^{-1}, \tag{8}$$

where N_{sp} the number of particle size classes.
It remains to discuss the equation of motion of such a tracer parcel k, which reads (Schneiderbauer *et al.*, 2016a, 2015b)

$$\frac{\mathrm{d}\boldsymbol{u}_{p,k}}{\mathrm{d}t} = \frac{1}{\tau_{c,k}} \left(\boldsymbol{u}_s - \boldsymbol{u}_{p,k} \right) + \boldsymbol{F}_k^{\mathrm{poly}} + \boldsymbol{g}, \tag{9}$$

where $\boldsymbol{u}_{p,k}$ denotes the velocity of the Lagrangian tracer parcel k, $\boldsymbol{u}_s$ the solids velocity, $\boldsymbol{g}$ the gravitational acceleration and $\tau_{c,k}$ is a collisional time scale required to accelerate a single particle to the average solids velocity (Syamlal *et al.*, 1993; Schneiderbauer *et al.*, 2016a, 2015b)

$$\frac{1}{\tau_{c,k}} = \frac{3(1+e)}{4} \varepsilon_s \left\| \boldsymbol{u}_{p,k} - \boldsymbol{u}_s \right\| \sum_j^{N_{sp}} \frac{x_j \left(d_{s,k} + d_{s,j} \right)^2 g_{0,kj}}{d_{s,k}^3 + d_{s,j}^3}. \tag{10}$$

Here, $e \approx 0.9$ is the coefficient of restitution, N_{sp} is defined in equation (8), $d_{s,j}$ the particle diameter of class j and x_j is defined in table 1. $g_{0,jk}$ denotes the radial distribution function, which accounts for the poly-disperse mixture of hard spheres (Iddir and Arastoopour, 2005). Note that equation (10) accounts for the contribution coming from the inter-particle stresses, i.e. inter-particle collisions. These are determined by the coarse-grained TFM solution and affect the trajectories of the tracer parcels by the collisional time scale $\tau_{c,k}$.
Since the tracers show different particle diameters $\boldsymbol{F}_k^{\mathrm{poly}}$ is the acceleration of a single particle of diameter $d_{s,k}$ within the local poly-disperse mixture of particles (units force per unit parcel mass, i.e. $\mathrm{m\,s^{-2}}$) due to the gas-solid drag force. Thus, the acceleration of parcel k due to the drag force can be written as (Schneiderbauer *et al.*, 2016a)

$$\boldsymbol{F}_k^{\mathrm{poly}} = \frac{1}{x_k \varepsilon_s \rho_s} \beta_k \left(\boldsymbol{u}_g - \boldsymbol{u}_{p,k} \right), \tag{11}$$

where $\widetilde{\beta}_k$ is presented in table 1. Note that here β_k is computed based on the Reynolds number computed from the local velocity of the tracer instead of the local velocity of the solid phase.

DIRECT REDUCTION OF IRON ORE

In the following, we briefly present the reduction model. For more details the reader is referred to Kinaci *et al.* (2017).

Species Transport and Heat Transfer

The local concentration of the reactant i is described by a transport equation for a corresponding species Y_i of the gas phase, which reads

$$\frac{\partial \varepsilon_g \rho_g Y_i}{\partial t} + \boldsymbol{\nabla} \cdot \left(\varepsilon_g \rho_g \boldsymbol{u}_g Y_i \right) = -\boldsymbol{\nabla} \varepsilon_g \boldsymbol{J}_i + \varepsilon_g \mathcal{R}_i, \tag{12}$$

where ρ_g is the density of the gas phase given by the equation of state for ideal gases and $\mathcal{R}_i$ accounts for net rate of generation/destruction of species i by chemical reactions. Finally, the diffusion flux $\boldsymbol{J}_i$ is written as

$$\boldsymbol{J}_i = -\rho_g D_{m,i} \boldsymbol{\nabla} Y_i - D_{T,i} \frac{\boldsymbol{\nabla} T_g}{T_g}, \tag{13}$$

where $D_{m,i}$ is the mass diffusion coefficient for species i and $D_{T,i}$ is the thermal (Soret) diffusion coefficient (ANSYS, 2011).
To describe the conservation of energy in fluidized bed reactors, a separate transport equation is solved for the specific enthalpy, h_q, of each phase:

$$\frac{\partial \varepsilon_q \rho_q h_q}{\partial t} + \boldsymbol{\nabla} \cdot \left(\varepsilon_q \rho_q \boldsymbol{u}_q h_q \right) = \boldsymbol{\Sigma}_q : \boldsymbol{\nabla} \boldsymbol{u}_q - \boldsymbol{\nabla} \cdot \boldsymbol{q}_q + \mathcal{S}_q + Q_{gs}, \tag{14}$$

where the heat flux $\boldsymbol{q}_q$ is modeled by using Fouriers law $\boldsymbol{q}_q = k_q \boldsymbol{\nabla} T_q$ and $\mathcal{S}_q$ accounts for the reaction heat. In case of the gas phase the heat conductivity k_g is computed employing a weighted average of the individual heat conductivities of the monomers. For the heat exchange between the gas and the solid phase, Q_{gs}, we employ the correlation proposed by Gunn (1978). Assuming constant specific heats $c_{p,q}$ the phase temperature and phase enthalpy are correlated as follows

$$h_q = c_{p,q} T_q. \tag{15}$$

Table 1: Summary of microscopic poly-disperse drag coefficient of Beetstra *et al.* (2007), which has been adapted in our previous work (Schneiderbauer *et al.*, 2015a). Here, $\bar{\varepsilon}_g$ denotes the filtered gas volume fraction, $\langle d_s \rangle$ the Sauter diameter, $\varepsilon_{s,i}$ the volume fraction of particle size class i and N_{sp} the number of particle size classes.

$$\widetilde{\beta} = 18\mu_g \bar{\varepsilon}_s \bar{\varepsilon}_g^2 F\left(\bar{\varepsilon}_s, \bar{\varepsilon}_g, \widetilde{\mathrm{Re}}_{\langle d_s \rangle}\right) \left(\sum_{i=1}^{N_{sp}} \frac{\bar{x}_i F_{\mathrm{poly}}(y_i)}{d_{s,i}^2} \right),$$

with

$$\widetilde{\mathrm{Re}}_{\langle d_s \rangle} = \frac{\bar{\varepsilon}_g \rho_g \langle d_s \rangle \|\widetilde{\boldsymbol{u}}_g - \widetilde{\boldsymbol{u}}_s\|}{\mu_g},$$

$$F_{\mathrm{poly}}(y_i) = \bar{\varepsilon}_g y_i + \bar{\varepsilon}_s y_i^2 + 0.064 \bar{\varepsilon}_g y_i^3,$$

$$F(\bar{\varepsilon}_s, \bar{\varepsilon}_g, \widetilde{\mathrm{Re}}_{\langle d_s \rangle}) = \frac{10\bar{\varepsilon}_s}{\bar{\varepsilon}_g^3} + \bar{\varepsilon}_g\left(1 + 1.5\bar{\varepsilon}_s^{1/2}\right) + \frac{0.413\widetilde{\mathrm{Re}}_{\langle d_s \rangle}}{24\bar{\varepsilon}_g^3} \left(\frac{\bar{\varepsilon}_g^{-1} + 3\bar{\varepsilon}_g\bar{\varepsilon}_s + 8.4\widetilde{\mathrm{Re}}_{\langle d_s \rangle}^{-0.343}}{1 + 10^{3\bar{\varepsilon}_s}\widetilde{\mathrm{Re}}_{\langle d_s \rangle}^{-(1+4\bar{\varepsilon}_s)/2}} \right)$$

and the dimensionless parameters

$$\bar{x}_i = \frac{\bar{\varepsilon}_{s,i}}{\bar{\varepsilon}_s}, \quad y_i = \frac{d_i}{\langle d_s \rangle}$$

Thermochemical Aspects

Modelling direct reduction of iron ore can be related to equilibrium phase diagrams. One such diagram demonstrates the reduction processes of the iron-oxygen-carbon system, which is also called the *Baur-Glaessner Diagram*. In this diagram, the stabilities for the iron-oxides and iron phases are depicted as a function of temperature and CO/CO_2 (H_2/H_2O) mixture with the available correlations for the equilibrium constant from literature and the ones calculated.

The concentration molar fraction of the relative gas species can be determined with the use of the equilibrium constant as

$$\frac{x_{CO_2}}{x_{CO}} = Ke_{\mathrm{Fe}_x\mathrm{O}_y,\,\mathrm{CO}}, \tag{16}$$

thus the molar fraction of the mixture can be defined with,

$$x_{CO_2} = k_c \frac{Ke_{\mathrm{Fe}_x\mathrm{O}_y,\,\mathrm{CO}}}{1 + Ke_{\mathrm{Fe}_x\mathrm{O}_y,\,\mathrm{CO}}} \tag{17}$$

or

$$x_{CO} = k_c \frac{1}{1 + Ke_{\mathrm{Fe}_x\mathrm{O}_y,\,\mathrm{CO}}}, \tag{18}$$

in which k_c represents the total content of carbon in the system that can be expressed with

$$x_{CO} + x_{CO_2} = k_c. \tag{19}$$

As a more advanced method one might consider a four-component gas mixture of CO, H_2, CO_2 and H_2O to be represented in a single Baur-Glaessner Diagram with an abscissa of $CO + H_2$ or $H_2O + CO_2$ content.

Reaction Kinetics

The most common types of representation models for the non-catalytic reactions of solids submerged in fluids is the shrinking particle model (SPM) and the unreacted shrinking core model (USCM) (Levenspiel, 1999), where the unreacted shrinking core model is accepted as the most precise model to represent direct reduction of iron ore (Valipour *et al.*, 2006; Valipour, 2009; Natsui *et al.*, 2014). In particular, the three layer unreacted shrinking core model developed by Philbrook, Spitzer and Manning (Tsay *et al.*, 1976) is able to represent the three interfaces of hematite/magnetite, magnetite/wustite and wustite/iron. For further details about the current implementation of the USCM the reader is referred to Kinaci *et al.* (2017).

According to Tsay *et al.* (1976) the removal rate of oxygen is determined through the following mechanisms: (i) The reducing gas is transported through the gas film onto the particle surface (F); (ii) diffusion through the porous iron layer (B_3); (iii) reactants react with wustite at the wustite/iron interface and form iron (A_3); (iv) remaining reactants diffuse through the wustite layer to the wustite/magnetite interface (B_2); (v) reaction with magnetite at layer surface forming wustite and gaseous products (A_2); (vi) remaining reactants diffuse through the magnetite layer to the magnetite/hematite interface (B_1); (vii) reaction with hematite core forming magnetite and a gaseous products (A_1); (viii) The gaseous products diffuses outwards through the pores of the pellet. Since each step is a resistance to the total reduction of the pellet, the reduction pattern of a single pellet can be considered to follow a resistance network such as an electrical resistance circuit network. The solution of this resistance network yields the reaction flow rate of $\dot{Y}_{j,i}$ of the gas species for the relative layers yields:

From hematite to magnetite:

$$\begin{aligned}\dot{Y}_{h,i} = &([A_3(A_2+B_2+B_3+F)+(A_2+B_2)(B_3+F)](Y-Y_1^{eq}) \\ &-[A_3(B_2+B_3+F)+B_2(B_3+F)](Y-Y_2^{eq}) \\ &-[A_2(B_3+F)](Y-Y_3^{eq}))\frac{1}{W_{3,i}},\end{aligned} \tag{20}$$

From magnetite to wustite:

$$\begin{aligned}\dot{Y}_{m,i} = &([(A_1+B_1+B_2)(A_3+B_3+F)+A_3(B_3+F)](Y-Y_2^{eq}) \\ &-[B_2(A_3+B_3+F)+A_3(B_3+F)](Y-Y_1^{eq}) \\ &-[(A_1+B_1)(B_3+F)](Y-Y_3^{eq}))\frac{1}{W_{3,i}},\end{aligned} \tag{21}$$

From wustite to iron:

$$\begin{aligned}\dot{Y}_{w,i} = &([(A_1+B_1)(A_2+B_2+B_3+F)+A_2(B_2+B_3+F)] \\ &(Y-Y_3^{eq})-[A_2(B_3+F)](Y-Y_1^{eq}) \\ &-[(A_1+B_1)(B_3+F)](Y-Y_2^{eq}))\frac{1}{W_{3,i}}\end{aligned} \tag{22}$$

where the index i denotes the gas-species i (i.e. either CO or H_2). Furthermore, A_j represents the relative chemical reaction resistance term, B_j the relative diffusivity resistance

term, j represents the layers hematite, magnetite and wustite and i the reducing gas species. F is the mass transfer resistance term, which is defined with $1/k_f$. Y is the bulk gas mole fraction and Y_j^{eq} the relative layer equilibrium mole fractions. The denominator $W_{3,i}$ is expressed as

$$W_{3,i} = [(A_1+B_1)(A_3(A_2+B_2+B_3+F)+(A_2+B_2)(B_3+F)) + A_2(A_3(B_2+B_3+F)+B_2(B_3+F))] \tag{23}$$

The chemical reaction resistance term $A_{j,i}$ can be expressed as

$$A_{j,i} = \left[\frac{1}{(1-f_j)^{\frac{2}{3}}} \frac{1}{k_j \left(1-\frac{1}{Ke_j}\right)} \right]_i \tag{24}$$

in which j represents the reduction layer, i the reducing gas, k the reaction rate constant and f_j is the local fractional reduction of the relative layer that is calculated as

$$f_j = 1 - \left(\frac{r_j}{r_g}\right)^3. \tag{25}$$

The diffusivity resistance term $B_{j,i}$ can be calculated for the relative iron oxide component as (Valipour *et al.*, 2006; Valipour, 2009)

$$B_{h,i} = \left[\frac{(1-f_m)^{\frac{1}{3}} - (1-f_h)^{\frac{1}{3}}}{(1-f_m)^{\frac{1}{3}}(1-f_h)^{\frac{1}{3}}} \frac{r_g}{De_h} \right]_i, \tag{26}$$

$$B_{m,i} = \left[\frac{(1-f_w)^{\frac{1}{3}} - (1-f_m)^{\frac{1}{3}}}{(1-f_w)^{\frac{1}{3}}(1-f_m)^{\frac{1}{3}}} \frac{r_g}{De_m} \right]_i, \tag{27}$$

$$B_{w,i} = \left[\frac{1-(1-f_w)^{\frac{1}{3}}}{(1-f_w)^{\frac{1}{3}}} \frac{r_g}{De_w} \right]_i, \tag{28}$$

in which De_j represents the diffusion coefficient of the relative layer.
With the use of the reaction flow rate $\dot{Y}_{j,i}$ the relative mass flow rates between layers can be defined as

$$\frac{dm_i}{dt} = C_i M_i A_p \dot{Y}_{j,i}. \tag{29}$$

Mass and Heat Transfer Coefficient

The mass transfer coefficient k_f which is used in the determination of the mass transfer term can be calculated through the Sherwood number or the Nusselt number as

$$Sh = \frac{k_f d}{D_e}, \qquad Nu = \frac{k_f}{k}, \tag{30}$$

where d is the diameter of pellet, D_e the diffusion coefficient and k the thermal conductivity. A number of correlations for determining the Sherwood number exist in literature. Lee and Barrow (Lee and Barrow, 1968) proposed a model through investigating the boundary layer and wake regions around the sphere leading to a Sherwood number of

$$Sh_t = (0.51Re^{0.5} + 0.02235Re^{0.78})Sc^{0.33}, \tag{31}$$

where Sc stands for the Schmidt number and defined as $\frac{\nu}{\rho D}$. In more recent works from Valipour (Valipour, 2009) and Nouri et al. (Nouri *et al.*, 2011) the Sherwood and Nusselt numbers are expressed as

$$Sh = 2 + 0.6Re^{0.5}Sc^{0.33}, \qquad Nu = 2 + 0.6Re^{0.5}Pr^{0.33}. \tag{32}$$

Pr represents the Prandtl number and is expressed as the specific heat times the viscosity over thermal conductivity $c\mu/k$. However, since fluidized beds usually show very dense regions we use the correlation proposed by Gunn (1978) to compute the Nusselt number and consequently the heat transfer coefficient.

Diffusivity Coefficient

Diffusivity of a gaseous species depends on properties such as the pore size distribution, void fraction and tortuosity. For example, according to Tsay *et al.* (1976) a pore size of 2μ to 5μ the Knudsen diffusion has been found to be 10 times faster than molecular diffusion, therefore in their work the Knudsen diffusion has been neglected, since slowest process mostly determines the final reaction rate. Thus, the effective binary gas diffusion was calculated with

$$D_{eff} = D_{12}\frac{\varepsilon}{\tau} \tag{33}$$

where ε represents the dimensionless void fraction, τ the tortuosity. (Valipour, 2009; Valipour *et al.*, 2006) has used the Fuller-Schettler-Giddings equation to determine the effective diffusivity as

$$D_{j,i} = \frac{10^{-7}T^{1.75}}{(P_t(\dot{v}_j^{1/3} + \dot{v}_i^{1/3}))^2}\left(\frac{1}{M_j} + \frac{1}{M_i}\right)^{0.5} \tag{34}$$

in which the $\dot{v}$ is the diffusion volume of the relative species, M is the molecular weight, P_t the total flow pressure and T the temperature in Kelvin.

Reaction Rate Coefficient

For many reactions the rate expression can be expressed as a temperature-dependent term. It has been established that in these kinds of reactions, the reaction rate constant can be expressed with the Arrhenius' law (Levenspiel, 1999) as follows

$$k = k_0 \exp\left(\frac{-E_a}{RT}\right), \tag{35}$$

in which k_0 represents the frequency factor or the pre-exponential factor, E_a the activation energy, R the universal gas constant and T the temperature. The values for the pre-exponential factor and the activation energy can be found through various works (Tsay *et al.*, 1976; Valipour, 2009).

IMPLEMENTATION

Since the motion equation of the Lagrangian particles (equation (9)) does only account for collision implicitly by using equation (10) the total volume fraction of the tracer particles, $\varepsilon_{s,p} = \sum_{i=1}^{N_{sp}} n_i \pi d_{s,i}^3/6$ (compare with equation (5)) may exceed the maximum packing locally. This, in turn, may yield an unphysical accumulation of tracer particles in dense regions. Thus, we introduce an additional repulsive mechanism $\boldsymbol{F}_k^{\text{pack}}$ (units $\mathrm{m\,s^{-2}}$), which prevents the Lagrangian tracer particles from forming dense aggregates exceeding the maximum packing fraction. Finally, the reduction model is evaluated at each parcel at each parcel time step. The resulting mass transfer and reaction heats have to be mapped to

the Eulerian grid to compute $\mathcal{R}_i$ (equations (3) and (12)) and $\mathcal{S}_q$ (equation (14)). For more details the reader is referred to equations (26) and (28) in our previous study (Schneiderbauer *et al.*, 2016b). Finally, it has to be noted that in the case where no tracer particle is in a specific numerical cell we apply a diffusive smoothening approach to the exchange fields locally (i.e. to the Sauter mean diameter; Pirker *et al.* (2011)).

For the numerical simulation we use the commercial finite volume CFD-solver FLUENT (version 16). For the discretization of all convective terms the QUICK (Quadratic Upwind Interpolation for Convection Kinematics) scheme is used. The derivatives appearing in the diffusion terms are computed by a least squares method and the pressure-velocity coupling is achieved by the phase coupled SIMPLE algorithm (Cokljat *et al.*, 2006). The trajectories of the Lagrangian tracer particles (equation (9)) is integrated after each fluid flow time step using a third-order Runge-Kutta method. Further it has to be noted that the gas velocity and the solid phase velocity in equation (9) are linearly interpolated to the particle positions by using a first order Taylor approximation. For fluidized bed simulations we employ a time step size of 0.001. More details on the implementation can be found in our previous studies (Schneiderbauer *et al.*, 2016a,b).

RESULTS

To validate the presented reduction model, we investigate the direct reduction of hematite ore within a lab-scale fluidized bed with 68 mm diameter (Spreitzer, 2016). The small dimensions of the vessel allow to use very fine grid spacings (i.e. ≈ 2 mm), which resolve all relevant heterogeneous structures, and therefore no sub-grid corrections are required (Schneiderbauer *et al.*, 2013; Schneiderbauer and Pirker, 2014). The pressure in the fluidized bed was 140000 Pa and the superficial gas velocity 0.25 m s^{-1}. The detailed process conditions are given in tables 2, 3 and 4. According to table 3 we use four different types of tracer parcel representing the different size fractions. In total we found that 120000 tracer parcels are appropriate to gather sufficient statistics (Schneiderbauer *et al.*, 2016a,b).

Table 2: Experimental conditions for the different reduction steps. The concentrations of the reactants are given in volume percent.

	R1 (W→Fe)	R2 (M→W)	R3 (H→M)
H_2	13.4%	15.9%	13.0%
H_2O	3.4%	6.8%	6.8%
CO	37.0%	37.4%	30.3%
CO_2	14.0%	27.4%	26.4%
N_2	32.2%	12.4%	23.5%
T[°C]	720	750	480

Table 3: Particle size distribution of the iron ore.

d_p	fraction [vol. %]
$0-0.063$	0
$0.063-0.125$	15.4
$0.125-0.25$	33.2
$0.25-0.5$	28.6
$0.5-1$	22.8

Figure 1 shows snapshots of the solid volume fraction, the mass fraction of CO, the mass fraction of CO_2 and the fractional reduction of individual parcels during the conversion of hematite to magnetite. On the one hand, figure 1a unveils that the bed is operated in the bubbling regime to optimize the solid mixing, the gas-solid contact as well as the reaction heat removal. On the other hand, figures 1b – 1d clearly reveal the removal of oxygen from the hematite ore due to the conversion of CO to CO_2, which increases the fraction reduction of the individual iron ore particles. In particular, the content of CO considerably decreases as the gas passes the particle bed while the content of CO_2 increases.

Table 4: Parameters for DRI-model (Hanel *et al.*, 2015).

		H→M	M→W	W→Fe
$\mathbf{H_2}$	k_0 [m/s]	160	29	6
	E_a [J]	68600	75000	65000
	Ke [-]	$e^{\frac{-362.6}{T_s}+10.334}$	$10^{\frac{-3577}{T_s}+3.74}$	$10^{\frac{-827}{T_s}-0.468}$
CO	k_0 [m/s]	437	45	17
	E_a [J]	102000	86000	68000
	Ke [-]	$e^{\frac{3968.37}{T_s}+3.94}$	$10^{\frac{-1834}{T_s}+2.17}$	$10^{\frac{914}{T_s}-1.097}$

Figure 2 shows the cumulative distribution function of the fractional reduction. The figure indicates that after about 150 s approximately 50% of the hematite ore was converted to magnetite. In particular, the smallest particles are already converted after 150 s while the larger particles still contain hematite (figure 3). This is clear, since the larger particles contain much more hematite ore than compared to their surface area than the smaller particles.

Finally, figure 4 shows the fractional reduction as a function of time for the different reduction steps. Both, experiment and simulation unveil that the conversion of hematite to magnetite (R3) is the fastest reduction step (Hanel *et al.*, 2015). After approximately 500 s the fractional reduction approaches a plateau, where the fractional reduction is about 11.1%. Here, the total amount of hematite was already converted to magnetite. The subsequent conversion from magnetite to wustite is known to be the second fasted reduction step, which is also correctly predicted by the presented conversion model. Again, the fractional reduction approaches a plateau region, where the fraction reduction is about 33.3%, which is in fairly good agreement with the experiment. It has to be noted that we stopped the simulations after reaching the plateau regions of fractional correction during R3 and R2 and extrapolated the fractional correction in time in figure 4 till the next reduction step to reduce the computational demands. The final reduction step, where wustite is converted to metallic iron, unveils the slowest conversion rate. This is also indicated by the kinetic parameters given in table 4. Similar to the previous reduction steps, the present model is able to correctly predict the conversion of wustite to iron.

CONCLUSION

We have presented the application of our previously published hybrid-TFM (Schneiderbauer *et al.*, 2015b; Schellander *et al.*, 2013; Pirker and Kahrimanovic, 2009; Schneiderbauer *et al.*, 2016a,b) to the conversion of iron ore to iron using fluidized bed technolgogy. Such a modelling strategy enables the efficient numerical analysis of reactive polydisperse gas-phase reactors without requiring computationally demanding multi-fluid models, which are coupled to population balance approaches.

To conclude, the results clearly show that the reactive hybrid-TFM is able to picture the correct conversion rates within the fluidized bed. Nevertheless, the conversion model has to

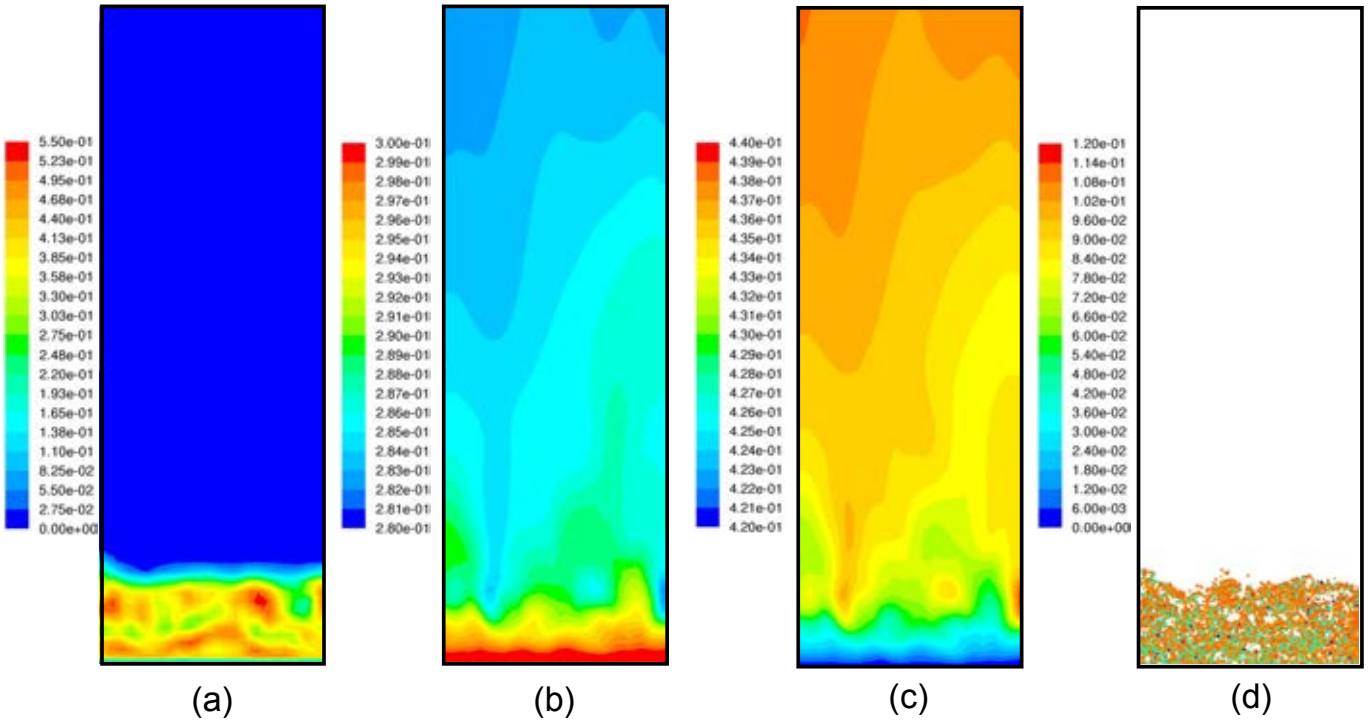

Figure 1: Snapshots at $t = 228$ s (i.e. within R_3) of a) the solid volume fraction, b) the mass fraction of CO, c) the mass fraction of CO_2 and d) the fractional reduction of individual parcels.

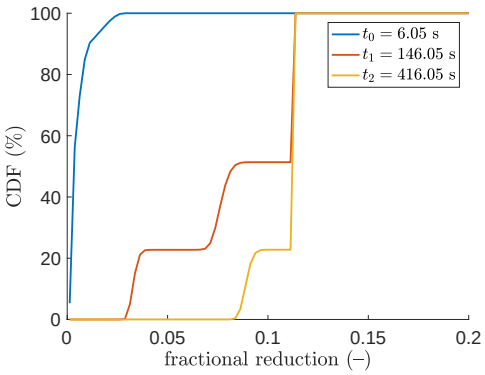

Figure 2: Snapshots of cumulative distribution of the fractional reduction during the conversion of hematite to magnetite.

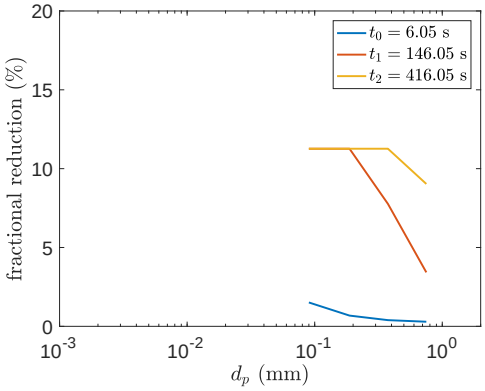

Figure 3: Snapshots of the fractional reduction as a function of the particle diameter during the conversion of hematite to magnetite.

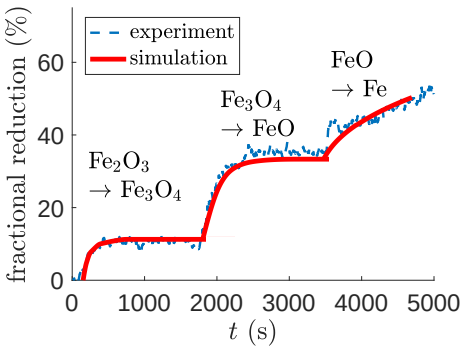

Figure 4: ractional reduction as a function of time for the different reduction steps.

be verified further against more different gas compositions. I.e. future efforts will concentrate on the numerical analysis of different process conditions and their detailed evaluation against experimental data. Finally, large-scale applications should be investigated, where sub-grid corrections will be required to account for the unresolved small scales on the behaviour of the fluidized bed and the conversion rates (Schneiderbauer, 2017).

ACKNOWLEDGEMENTS

The authors want to acknowledge the support of Dr. Christoph Klaus-Nietrost, who provided the c-code for the reduction model developed during his PhD work *"Development of Conversion Models for Iron-Carriers and Additives within a Melter-Gasifier or Blast Furnace"* (Institute for Energy Systems and Thermodynamics, TU Vienna, 2016). This work was funded by the Christian-Doppler Research Association, the Austrian Federal Ministry of Economy, Family and Youth, and the Austrian National Foundation for Research, Technology and Development. The author also wants to acknowledge the financial support from the K1MET center for metallurgical research in Austria (www.k1-met.com).

REFERENCES

AGRAWAL, K., LOEZOS, P.N., SYAMLAL, M. and SUNDARESAN, S. (2001). "The role of meso-scale structures in rapid gas-solid flows". *Journal of Fluid Mechanics*, **445**, 151–185.

ANSYS (2011). *ANSYS FLUENT Theory Guide*, vol. 15317. ANSYS, Inc., Canonsburg, PA.

BEETSTRA, R., Van der Hoef, M.A. and KUIPERS, J.A.M. (2007). "Drag Force of Intermediate Reynolds Number Flow Past Mono- and Bidisperse Arrays of Spheres". *AIChE Journal*, **53(2)**, 489–501.

COKLJAT, D., SLACK, M., VASQUEZ, S.A., BAKKER, A. and MONTANTE, G. (2006). "Reynolds-Stress Model for Eulerian multiphase". *Progress in Computational Fluid Dynamics, An International Journal*, **6(1/2/3)**, 168.

FU, D., ZHOU, C.Q. and CHEN, Y. (2014). "Numerical Methods for Simulating the Reduction of Iron Ore in Blast Furnace Shaft". *Journal of Thermal Science and Engineering Applications*, **6(2)**, 021014.

GONIVA, C., KLOSS, C., DEEN, N.G., KUIPERS, J.A.M. and PIRKER, S. (2012). "Influence of rolling friction on single spout fluidized bed simulation". *Particuology*, **10(5)**, 582–591.

GUNN, D.J. (1978). "Transfer of Heat or Mass to Particles in Fixed and Fluidized Bed". *International Journal of Heat Mass Transfer*, **21**, 467–476.

HABERMANN, A., WINTER, F., HOFBAUER, H., ZIRNGAST, J. and SCHENK, J.L. (2000). "An Experimental Study on the Kinetics of Fluidized Bed Iron Ore Reduction". *ISIJ International*, **40(10)**, 935–942.

HANEL, M.B., SCHENK, J.F., MALI, H., HAUZENBERGER, F., THALER, C. and STOCKER, H. (2015). "Characterization of Ferrous Burden Material for Use in Ironmaking Technologies". *BHM Berg- und Hüttenmännische Monatshefte*, **160(7)**, 316–319.

HRENYA, C.M. and SINCLAIR, J.L. (1997). "Effects of particle-phase turbulence in gas-solid flows". *AIChE Journal*, **43(4)**, 853–869.

IDDIR, H. and ARASTOOPOUR, H. (2005). "Modeling of multitype particle flow using the kinetic theory approach". *AIChE Journal*, **51(6)**, 1620–1632.

KINACI, M.E., LICHTENEGGER, T. and SCHNEIDERBAUER, S. (2017). "Modelling of Chemical Reactions in Metallurgical Processes". J.E. Olsen (ed.), *Proceedings of the 12th International Conference on Computational Fluid Dynamics in the Oil & Gas, Metallurgical and Process Industries (CFD 2017)*. SINTEF, Trondheim, Norway, Trondheim, Norway.

LEE, K. and BARROW, H. (1968). "Transport processes in flow around a sphere with particular reference to the transfer of mass". *International Journal of Heat and Mass Transfer*, **11(6)**, 1013–1026.

LEVENSPIEL, O. (1999). *Chemical Reaction Engineering*.

LUN, C.K.K., SAVAGE, S.B., JEFFREY, D.J. and CHEPURNIY, N. (1984). "Kinetic theories for granular flow: inelastic particles in Couette flow and slightly inelastic particles in a general flowfield". *Journal of Fluid Mechanics*, **140**, 223–256.

NATSUI, S., KIKUCHI, T. and SUZUKI, R.O. (2014). "Numerical Analysis of Carbon Monoxide-Hydrogen Gas Reduction of Iron Ore in a Packed Bed by an Euler-Lagrange Approach". *Metallurgical and Materials Transactions B*, **45(6)**, 2395–2413.

NOURI, S.M.M., Ale Ebrahim, H. and JAMSHIDI, E. (2011). "Simulation of direct reduction reactor by the grain model". *Chemical Engineering Journal*, **166(2)**, 704–709.

PIRKER, S. and KAHRIMANOVIC, D. (2009). "Modelling Mass Loading Effects in Industrial Cyclones by a Combined Eulerian-Lagrangian Approach". *Acta Mechanica*, **204(2)**, 203–216.

PIRKER, S., KAHRIMANOVIC, D., KLOSS, C., POPOFF, B. and BRAUN, M. (2010). "Simulating coarse particle conveying by a set of Eulerian, Lagrangian and hybrid particle models". *Powder Technology*, **204(2-3)**, 203–213.

PIRKER, S., KAHRIMANOVIC, D. and GONIVA, C. (2011). "Improving the applicability of discrete phase simulations by smoothening their exchange fields". *Applied Mathematical Modelling*, **35(5)**, 2479–2488.

PLAUL, F.J., BÖHM, C. and SCHENK, J.L. (2009). "Fluidized-bed technology for the production of iron products for steelmaking". *Journal of the Southern African Institute of Mining and Metallurgy*, **109(2)**, 121–128.

Primetals Technologies Austria GmbH and POSCO E&C (2015). "The finex® process – economical and environmentally safe ironmaking". `http://www.primetals.com/en/technologies/ironmaking/finex%C2%AE/Lists/FurtherInformation/The%20Finex%20process.pdf`. Accessed: 2017-02-28.

RADL, S. and SUNDARESAN, S. (2014). "A drag model for filtered Euler-Lagrange simulations of clustered gas-particle suspensions". *Chemical Engineering Science*, **117**, 416–425.

SCHELLANDER, D., SCHNEIDERBAUER, S. and PIRKER, S. (2013). "Numerical study of dilute and dense poly-dispersed gas-solid two-phase flows using an Eulerian and Lagrangian hybrid model". *Chemical Engineering Science*, **95**, 107–118.

SCHENK, J.L. (2011). "Recent status of fluidized bed technologies for producing iron input materials for steelmaking". *Particuology*, **9(1)**, 14–23.

SCHNEIDERBAUER, S. (2017). "A spatially-averaged two-fluid model for dense large-scale gas-solid flows". *AIChE Journal*.

SCHNEIDERBAUER, S. and PIRKER, S. (2014). "Filtered and heterogeneity based sub-grid modifications for gas-solid drag and solids stresses in bubbling fluidized beds". *AIChE Journal*, **60(3)**, 839–854.

SCHNEIDERBAUER, S., AIGNER, A. and PIRKER, S. (2012). "A comprehensive frictional-kinetic model for gas-particle flows: analysis of fluidized and moving bed regimes". *Chemical Engineering Science*, **80**, 279–292.

SCHNEIDERBAUER, S., PUTTINGER, S. and PIRKER, S. (2013). "Comparative Analysis of Subgrid Drag Modifications for Dense Gas-Particle Flows in Bubbling Fluidized Beds". *AIChE Journal*, **59(11)**, 4077–4099.

SCHNEIDERBAUER, S., PUTTINGER, S., PIRKER, S., AGUAYO, P. and KANELLOPOULOS, V. (2015a). "CFD Modeling and Simulation of Industrial Scale Olefin Polymerization Fluidized Bed Reactors". *Chemical Engineering Journal*, **264**, 99–112.

SCHNEIDERBAUER, S., PUTTINGER, S. and PIRKER, S. (2015b). "Numerical study of a bi-disperse gas-solid fluidized bed using an Eulerian and Lagrangian hybrid model". *Procedia Engineering*, **102**, 1539–1545.

SCHNEIDERBAUER, S., HAIDER, M.F., HAUZENBERGER, F. and PIRKER, S. (2016a). "A Lagrangian-Eulerian Hybrid Model for the Simulation of Industrial-scale

Gas-solid Cyclones". *Powder Technology*, **304**, 229—-240.

SCHNEIDERBAUER, S., PIRKER, S., PUTTINGER, S., AGUAYO, P., TOULOUPIDIS, V. and Martínez Joaristi, A. (2016b). "A Lagrangian-Eulerian Hybrid Model for the Simulation of Poly-disperse Fluidized Beds: Application to Industrial-scale Olefin Polymerization". *Powder Technology (in press)*.

SPREITZER, D. (2016). *Optimierung der Prozessparameter für die Reduktion von Feineisenerzen mittels Wirbelschichtverfahren*. Master thesis, Montanuniversität Leoben.

SYAMLAL, M., ROGERS, W. and O'BRIEN, T.J. (1993). "MFIX documentation theory guide, Technical note". Tech. Rep. December, U.S. Department of Energy, Office of Fossil Energy, Morgantown, West Virginia.

TSAY, Q.T., RAY, W.H. and SZEKLEY, J. (1976). "The modeling of hematite reduction with hydrogen plus carbon monoxide mixture". *AIChE J*, **22(6)**, 1064–1076.

VALIPOUR, M.S. (2009). "Mathematical Modeling of a Non-Catalytic Gas-Solid Reaction : Hematite Pellet Reduction with Syngas". *Transactions C: Chemistry and Chemical Engineering*, **16(2)**, 108–124.

VALIPOUR, M.S., Motamed Hashemi, M.Y. and SABOOHI, Y. (2006). "Mathematical modeling of the reaction in an iron ore pellet using a mixture of hydrogen, water vapor, carbon monoxide and carbon dioxide: an isothermal study". *Advanced Powder Technology*, **17(3)**, 277–295.